CEMENT and CONCRETE RESEARCH. Vol. 17, pp. 441-452. Printed in the USA.
0008-8846/87 $3.00+00. Copyright (c) 1987 Pergamon Journals, Ltd.

EXPERIMENTAL DETERMINATION OF THE TENSION-SOFTENING RELATIONS FOR CEMENTITIOUS COMPOSITES

Victor C. Li , Chun-Man Chan and Christopher K.Y. Leung
Department of Civil Engineering
Massachusetts Institute of Technology
Cambridge, MA 02139

(Communicated by Z.P. Bazant)
(Received Oct. 1, 1986)

ABSTRACT

A novel experimental techique based on the J-integral is employed to experimentally determine the tension-softening (σ–δ) relations in cementitious composites. The σ–δ relation provides information on fracture resistance and could be used for numerical simulations of crack formation and propagation in structures constructed from materials which exhibit "tension-softening" behavior. With this method, no complicated modifications to testing machines are required. In the experiment, two pre-cracked specimens with slightly different notch lengths are used. The corresponding values of load, load point displacement and crack tip separation are simultaneously recorded. From this experimental data, the J-integral as a function of crack tip separation as well as the tension-softening curve can be deduced. These curves also provide a measure of the critical energy release rate. The experimental technique has been applied to mortar. It is suggested that the relatively simple technique can provide reliable material parameters for characterization of fracture resistance in plain and fiber reinforced cementitious composites independent of specimen geometry, size and loading configurations.

INTRODUCTION

The need for characterizing fracture resistance in concrete is well established. Fracture resistance characterization is needed for material toughness or ductility ranking and for design against fracture and cracking failure in concrete structures. The K_{Ic}-test standard for many brittle materials, however, has been recognized to be inadequate for toughness testing in concrete. This is because of the size-dependence of the apparent fracture toughness resulting from specimens of typical laboratory size, due to the relatively large process zone in comparison to other characteristic planar dimensions of the specimen. For this reason, a valid K_{Ic}-test requires impractically large specimen sizes [1,4].

The tension-softening (σ–δ) relation is defined as the functional relationship between the traction acting across a crack plane and the separation distance of the crack faces, in a uniaxial tension specimen loaded quasi-statically to complete failure. The σ–δ relation contains information on the tensile strength f_t, the critical separation distance δ_c, and the critical energy release rate G_c under the small scale yielding condition [2]. In addition, with the σ–δ relation, fracture analysis may be performed even when linear elastic fracture mechanics (LEFM) is inapplicable [3,4,11]. Li & Liang [3] describes the transition of validity from LEFM to non-linear elastic fracture mechanics to simple strength concept. Hillerborg [4] suggests the use of the σ–δ relation in analyzing crack formation and propagation in structures. Furthermore, when G_c is deduced from an experimentally determined σ–δ curve which involves no assumption of LEFM, G_c may be expected to be size-independent even if the specimen used to determine the σ–δ curve is small. Thus the σ–δ relation is a very useful basic 'parameter' characterizing fracture

resistance in cementitious composites.

Attempts at measuring σ–δ curve using direct uniaxial tension tests have met with various successes [5,6,7,8]. An inherent difficulty with the direct tension test is the stability of loading the specimen during the softening process, which is the main focus of the test. Often modification of the machine is necessary to stiffen the loading system. Even then, problems related to load eccentricity, crack location(s), effects of strain gauge length and elastic unloading make the uniaxial tension test difficult to perform.

In this paper, we present some results on measuring the curve for mortar, based on a technique briefly introduced by Li [2], which eliminates the problems mentioned above. The theory behind the technique is summarized in the following section. The experimental set-up will then be described. The data analysis procedure as well as test results for mortar and comparisons with available independent test data are reported next. While further tests are being conducted, we regard the preliminary results as encouraging in confirming the validity of the theoretical concepts and the advantages of this technique.

THEORETICAL BASIS OF EXPERIMENTAL TECHNIQUE

Rice [9] showed that the path-independent J-integral defined as

$$J = \int_{\Gamma} [W dy - T_i (du_i/dx) ds] \qquad (1)$$

where W is the elastic strain energy density, T_i is the traction vector, u_i is the displacement vector, and other quantities are defined in Fig. 1a, may be interpreted as the potential energy (PE) change per unit crack advance in a linear elastic body. Hence

$$J = - \partial(PE)/\partial a \qquad (2)$$

where a is the length of the crack, and the minus sign in (2) indicates a decrease in potential energy when the crack extends in length under fixed grip condition.

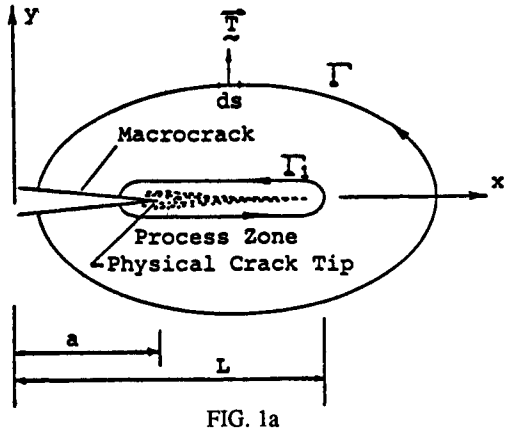

FIG. 1a
J-Integral Contours around Crack Tip

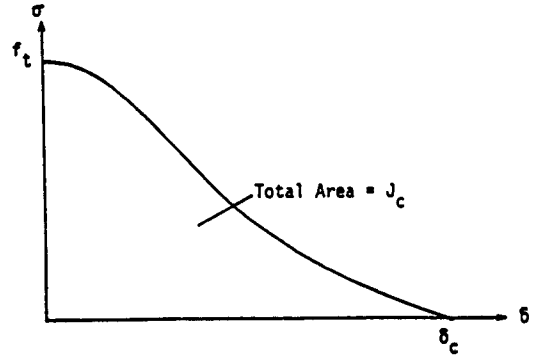

FIG. 1b
A Typical Tension-Softening Curve

We now specialize the J-integral for a material which exhibits localized inelastic deformation on a plane ahead of the crack tip. If we shrink the general contour Γ onto Γ_1 running alongside the process zone, as shown in Fig. 1a, it can be shown [9,10] that Eq. (1) reduces to

$$J = - \int_a^L \sigma(x) \, (\partial\delta/\partial x) \, dx \qquad (3)$$

where σ(x) and δ(x) are the normal stress and opening displacement at the point x in the process zone. The upper integral limit L is measured to a point x ahead of the physical crack tip where δ(x) = 0. Changing variables from x to δ, and since σ is a single valued function of δ (i.e. for each δ, there corresponds a unique value of σ in the σ–δ relation, Fig 1b),

$$J(\delta) = \int_0^{\delta} \sigma(\delta)\, d\delta \qquad (4)$$

A critical value of $J = J_c$ is reached when the separation δ at the physical crack tip reaches δ_c. In this case J_c may be interpreted as the complete area under the tension-softening curve (Fig. 1b) and δ_c is the material separation at which the load carrying capacity just vanishes. In the special case where the process zone size (L-a) is much smaller than all other planar dimensions in the problem, J_c and the critical energy release rate G_c coincide [9]. Equation (4) may be regarded as a specialization of (1) under the assumptions of a localized planar process zone in which the tensile stress decays from f_t to zero as the opening increases from zero to δ_c. The σ–δ curve, however, does not need to observe the small scale yielding condition of LEFM and is thus a more fundamental material property than G_c.

Since the potential energy change may be obtained from a global load deformation curve, J may be readily determined experimentally. To illustrate, for a compact tension specimen loaded with load level P and load point displacement Δ, as shown in Fig. 2, Eq. (2) implies

$$J(\Delta) = -(1/B) \int_0^{\Delta} (\partial P/\partial a)_{\Delta'}\, d\Delta' \qquad (5)$$

where B is the thickness of the specimen and the minus sign indicates a potential energy decrease when the crack advances at fixed load point displacement Δ. Since crack tip positions are difficult to locate accurately, it would be next to impossible to directly evaluate (5) by propagating a crack in a single specimen. An approximate procedure is to use two specimens identical in every respect except for a small difference in notch length (a_2-a_1) as shown in Fig. 2a and 2b. In this case, (5) may be interpreted as the area between the P-Δ curves for each of the two specimens, i.e.

$$J(\Delta) = (1/B)\,[\,\text{Area}\,(\Delta) / (a_2 - a_1)\,] \qquad (6)$$

Since a_1 and a_2 are pre-cut (or casted) notch lengths, there should be no difficulty calculating $J(\Delta)$. It may be expected that $J(\Delta)$ increases from zero and asymptotically approaches J_c.

If J_c is all we want, then (6) is already adequate. If we want to deduce the tension-softening relation, Eq. (4) may be utilized, since by differentiation,

$$\sigma(\delta) = \partial J(\delta)/\partial\delta \qquad (7a)$$

and combining with (6)

$$\sigma(\delta) = \{1/[B(a_2 - a_1)]\}[\partial\, \text{Area}\,(\Delta) / \partial\delta\,] \qquad (7b)$$

To use Eq. (7) effectively, Δ and δ must be correlated. This can be done by recording the opening at the crack tip during the loading process. Thus the experimental outputs required to obtain $\sigma(\delta)$ are a set of P-Δ and P-δ relations for each type of specimen with different notch lengths. While $(a_2 - a_1)$ should be as close to zero as possible in principle, experimental accuracy and material variability put a lower limit on this value.

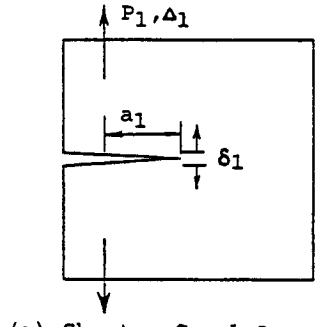

(a) Shorter Crack Length Specimen

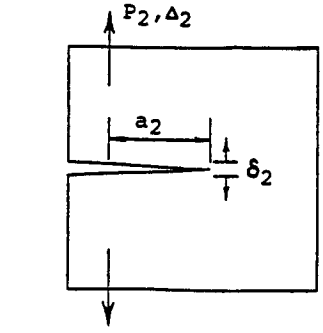

(b) Longer Crack Length Specimen

FIG. 2
Compliance Test Specimen

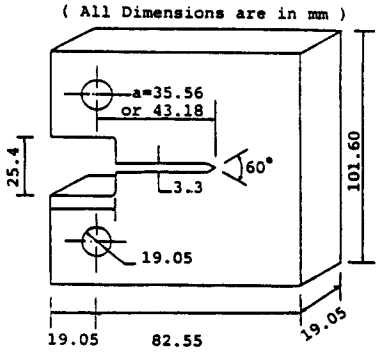

FIG. 3
Configuration of
Compact Tension Specimen

EXPERIMENTAL SET-UP

Specimen Specifications and Preparation:

The compact tension specimen dimensions are shown in Fig. 3. The two types of specimens differ only in their notch lengths by 7.62 mm.

For this preliminary study, we have chosen a mortar with composition shown in Table 1.

These specimens are prepared using a plexi-glass mould shown in Fig. 4a, with the notches casted in by two sets of teeth of a stiff aluminum bar. After curing, the aluminum bar with the teeth was removed by the screw action (Fig. 4b). This preparation procedure ensures uniformity of the two types of specimens, and also avoids damages which may be introduced by cutting the specimens and notches. More details in specimen preparation can be found in [10].

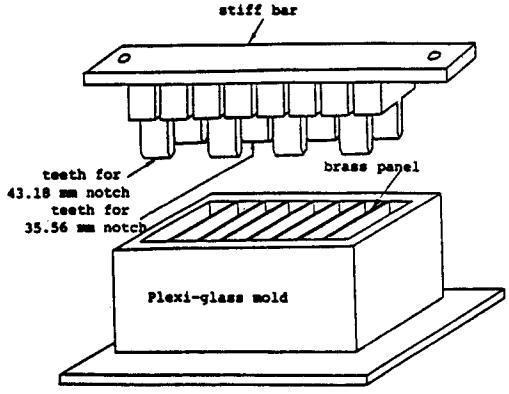

FIG. 4a
Compact Tension Test Specimen Mould

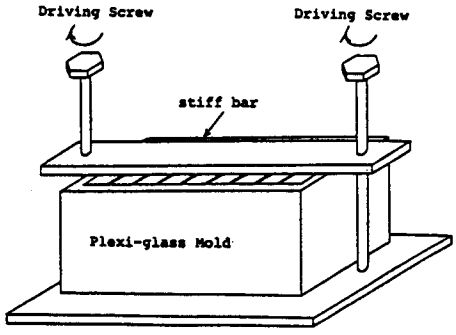

FIG. 4b
Removal of Test Specimens from Mould

TABLE 1
Material Specification of the Present Investigation

Cement Type:	Type III portland cement
Aggregate Type:	Seive No. 10 crushed stone sand nominal dimension = 2.004 mm
Water/Cement Ratio:	0.5
Cement:	311 kg/m^3
Aggregate:	622 kg/m^3
Water:	155.5 kg/m^3
Age:	7 days

Instrumentation and Equipment Set-Up:

A photograph of the experimental set-up is shown in Fig. 5. Details of the instrumentation scheme is shown in Fig. 6. Apart from the load and load point displacement measurements, the most important piece of information is the crack tip material separation. This separation (as well as the load point displacement) was measured by means of a non-contacting proximity sensor system illustrated in Fig. 7. These displacement measuring devices use an inductive operating principle to measure the distance between the proximity sensor tip and the metallic target (made of aluminum). This distance controls an oscillator's amplitude, which provides an analog signal proportional to displacement. The advantages of using these proximity sensors include the high accuracy (with resolution of .1μm) and extreme stability (insensitivity to environmental changes). The detailed arrangement of the proximity sensors and targets is shown in Fig. 8. Further details of sensor calibration and equipment set-up can be found in [10].

FIG. 5
Photograph of
Experimental Set-up

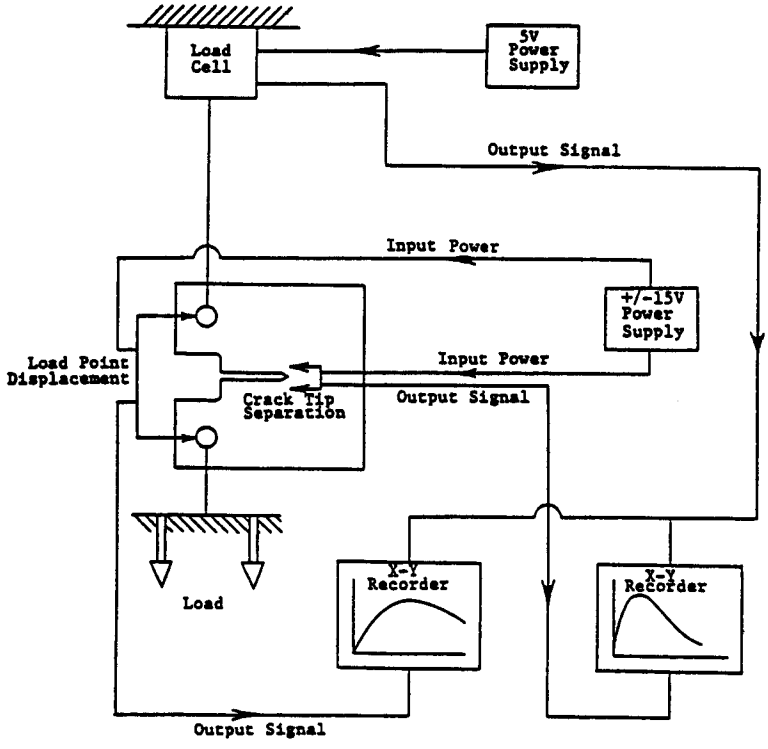

FIG. 6
Illustration of Instrumentation Scheme

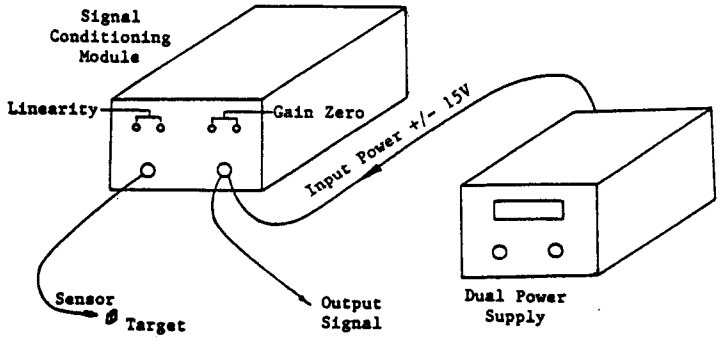

FIG.7
Displacement Measuring System

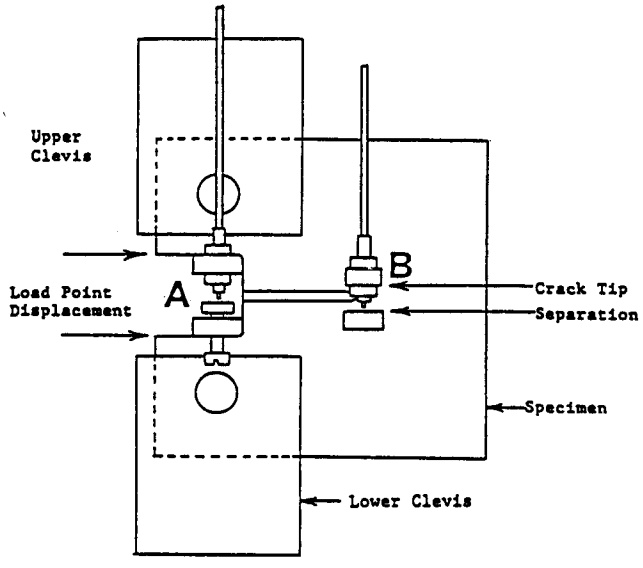

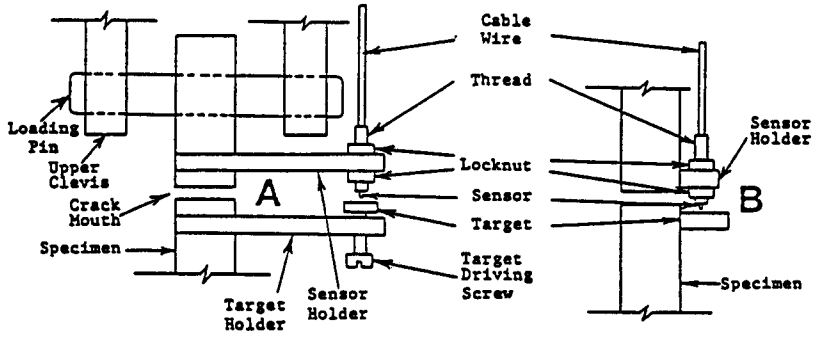

FIG. 8
Arrangement for Test Specimen

RESULTS AND DATA ANALYSIS PROCEDURE

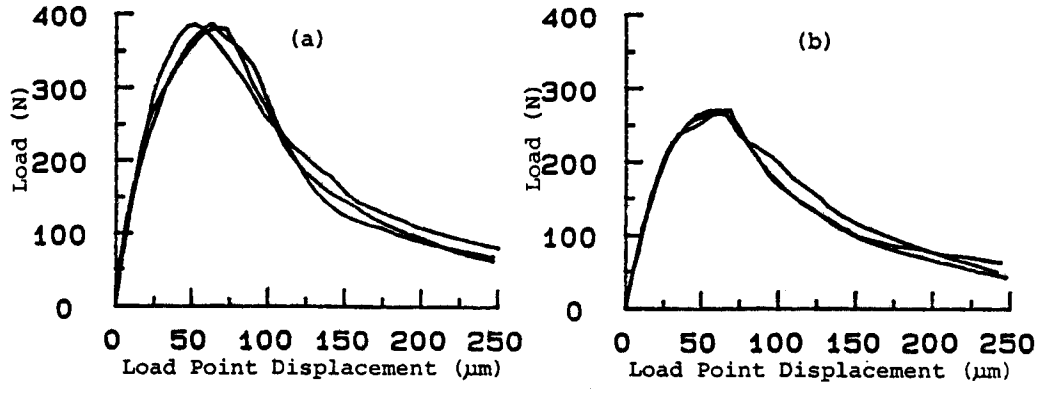

FIG. 9
Load vs Load Point Displacement Raw Data for (a) 35.56mm notch depth and (b) 43.18mm notch depth

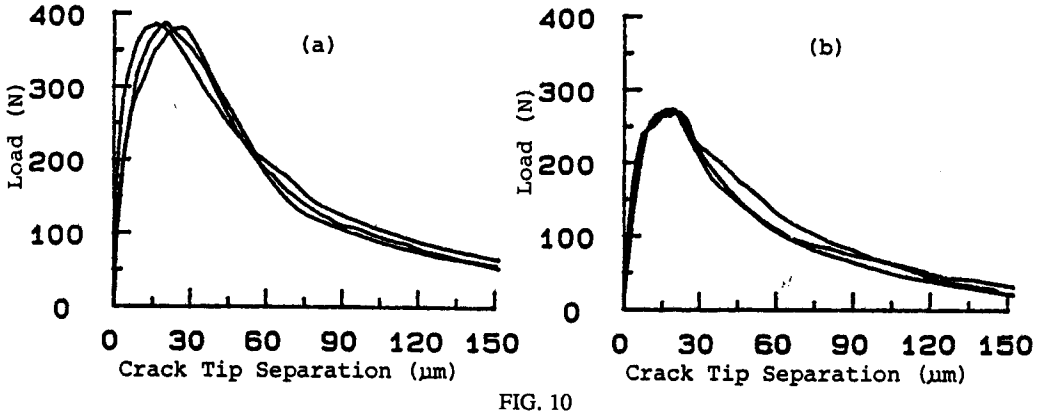

FIG. 10
Load vs Crack Tip Separation Raw Data for (a) 35.56 mm notch depth and (b) 43.18mm notch depth

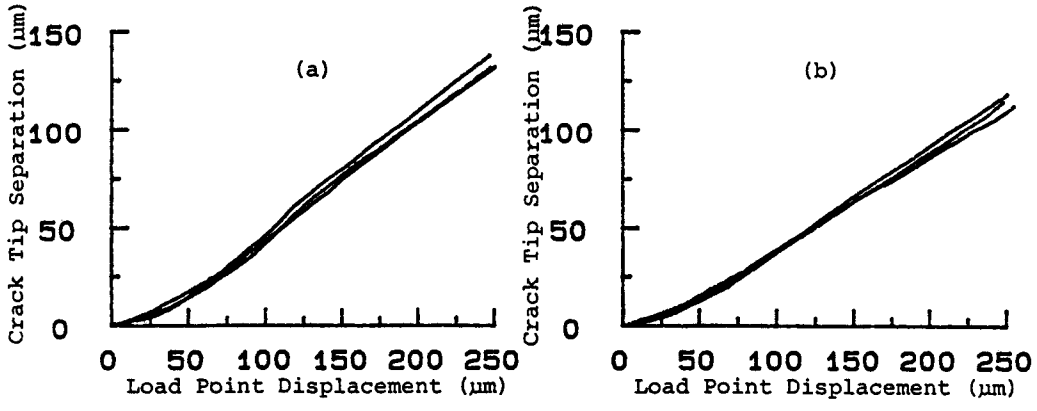

FIG.11
Crack Tip Separation vs Load Point Displacement Raw Data for (a) 35.56mm notch depth
(b) 43.18mm notch depth

The raw data are in terms of P vs. Δ and P vs δ curves as shown in Figs 9a,b and 10a, b. Each test is repeated at

least four times and the three most consistent results are adopted for averaging by regression techniques. From points corresponding to the same value of P on the P-Δ and P-δ curves, data sets of δ vs Δ are obtained. These are shown in Figs. 11a and 11b.

The data analysis procedure can be summarized in the following steps:

1. Functions of the form (polynomial in Δ) * exp(-bΔ) (where b is a constant) are fitted to the P-Δ curves for both types of specimens.

   For a = 35.56 mm $P = P_1(\Delta)$
   a = 43.18 mm $P = P_2(\Delta)$ (Fig. 12)

2. A polynomial is fitted to the δ–Δ data points for each specimen

   For a = 35.56 mm $\delta = \delta_1(\Delta)$
   a = 43.18 mm $\delta = \delta_2(\Delta)$ (Fig. 13)

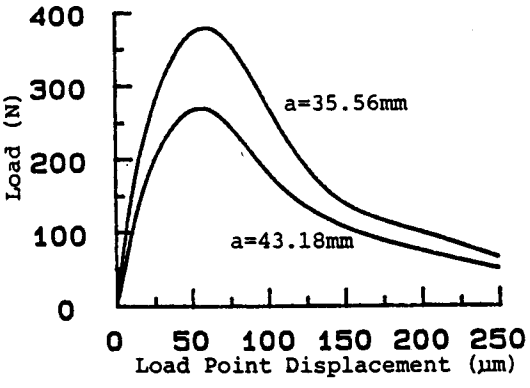

FIG. 12
Load vs Load Point Displacement
Regressed Curves

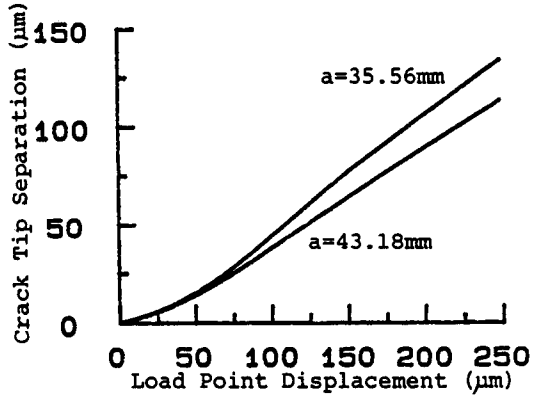

FIG. 13
Crack Tip Separation vs Load Point Displacement
Regressed Curves

3. For a given value of Δ,

$$J(\Delta) = \{1/[B(a_2 - a_1)]\} \int_0^{\Delta} [P_1(\Delta') - P_2(\Delta')]\, d\Delta' \qquad \text{(From Eqn. 6)}$$

   and we take

$$\delta(\Delta) = [\, \delta_1(\Delta) + \delta_2(\Delta) \,] / 2$$

   Hence, a new data set of J vs δ is obtained.

4. A function is fitted to the J-δ values as obtained above, taking into consideration the following points:
   (i) As δ increases, J will approach a constant value J_c.
   (ii) At δ=0, J=0. This is obvious since when δ is zero, both P_1 and P_2 are zero.
   (iii) At δ=0, $\partial J/\partial \delta = 0$.

The third point needs more detailed explanation. Note that

$$\partial J/\partial \delta = (\partial J/\partial \Delta) \;/\; (\partial \delta/\partial \Delta)$$

At $\delta = \Delta = 0$, $\partial J/\partial \Delta = \{1/[B(a_2 - a_1)]\}\, [\, P_1(\Delta) - P_2(\Delta) \,] = 0$ (since $P_1(\Delta) = P_2(\Delta) = 0$)
Theoretically, at δ=0, $\partial \delta/\partial \Delta$ should also be zero because when Δ first increases from zero, the tensile strength has not yet been reached at the crack tip and thus there is no crack separation. In other words,

$\partial\delta=0$ and thus $\partial\delta/\partial\Delta = 0$. However, in practice, in order to measure δ, we must put our measuring equipment and its target on two holders at opposite sides of the crack. As Δ increases from zero, the holders will move apart from each other and what we get for δ is actually the average strain times the distance between the holders. Therefore $\partial\delta/\partial\Delta$ obtains a finite value even at $\delta=0$. Hence $\partial J/\partial\delta$ = (zero / a finite value) = 0.

With the above mentioned constraints in mind, the J-δ values are fitted with a function of the form

$$J(\delta) = a - (a + a^*p^* \delta + b^*\delta^2 + c^*\delta^3) \,^*\exp(-p^*\delta)$$

The result is shown in Fig. 14.

5. $J(\delta)$ is then differentiated with respect to δ to obtain the σ–δ curve on Fig. 15. Note that the deduced σ–δ curve rises to a peak initially, then decreases as expected with increasing δ. The rising portion is due to the presence of strain between the instrument holders. It can be interpreted as sum of the elastic energy stored and the distributed damage (microcracking) prior to localization of inelastic deformation onto the fracture process zone, and therefore should not be regarded as part of the σ–δ relation. Fig. 16 shows the corrected σ–δ curve.

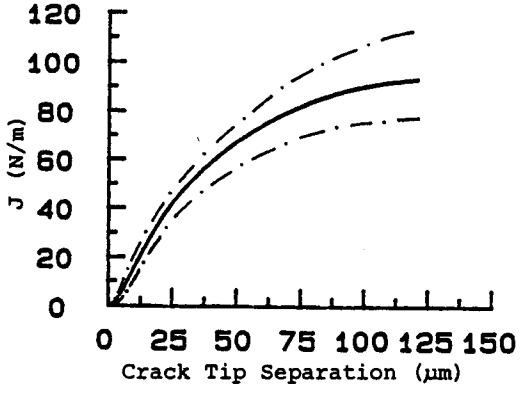

FIG. 14
The J vs Crack Tip Separation Curve
(Dot-Dash Line shows Upper & Lower Bounds)

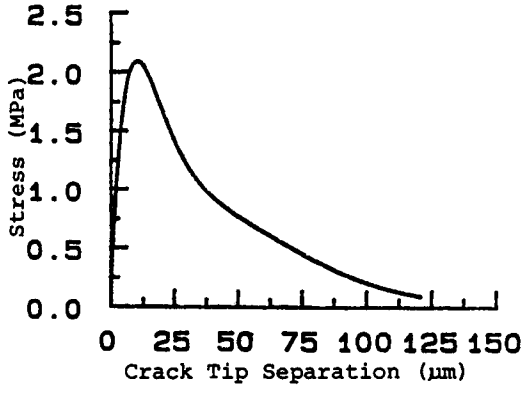

FIG. 15
The Deduced Tension-Softening Curve

FIG. 16
The Corrected Tension-Softening Curve
(Dot-Dash Curves show Upper & Lower Bounds
Dotted Part is Extrapolation of tension-softening Curve)

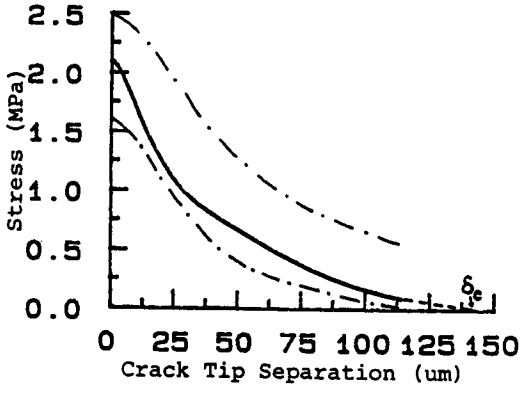

As we have three sets of data for each crack length, if we fit an expression to each of the individual curves and proceed as above, nine separate J-δ curves and σ–δ curves can be obtained. An upper bound and a lower bound can then be drawn to envelope those curves. These bounds are shown in Fig. 14 and Fig. 16 to give an idea of the deviation of raw data from the best fit.

In Fig. 16, the σ–δ curve is extrapolated to obtain the critical crack separation. This is shown as the dotted line. In future tests, data recording should continue until the P–Δ curves for the long notch length specimens join with those for the short notch length specimens. For this set of test, the material properties f_t, G_c, δ_c and l_{ch} ($=E_cG_c/f_t^2$) are summarized in the first row of Table 2. The value of initial elastic modulus E_c (from direct compression tests) is also given as a reference of the quality of the mortar tested.

TABLE 2
Comparison of Different Test Results

Reference	* Initial Elastic Modulus E_c (GPa)	** Tensile Strength f_t (MPa)	*** Fracture Energy G_c (N/m)	Critical Separation δ_c (μm)	**** Characteristic Length l_{ch} (cm)
(1) This investigation	27.0	2.09	83.8	139.7	51.80
(2) Evans & Marathe[5]	18.1	2.10	29.1	43.7	11.94
(3) Petersson [6]	41.7	3.61	115.9	178.6	37.09
(4) Gopalaratnam & Shah [7]	30.2	3.35	83.5	112.0	22.47
(5) Reinhardt [8]	33.2	3.49	144.1	238.4	39.28

* The initial elastic modulus of this investigation was calculated from the direct compression test: those of the other investigations were calculated from their given stress-deformation curves.
** Calculated from area below tension-softening curve.
*** Estimated value from extrapolation.
**** To compare with other results, this value has to be corrected as described in the text.

VERIFICATION OF EXPERIMENTAL RESULTS

Direct comparison of the tension-softening relation deduced by our technique with those by direct tension tests performed by other researchers [5,6,7,8] is met with difficulties since material compositions are different. However, a comparison in normalized form (with σ normalized by f_t and δ by l_{ch}) is shown in Fig. 17.

Instead of the l_{ch} in Table 2, we used a corrected value for l_{ch} to account for the difference in age of our specimen (7 days) and those of other investigators (28 days). It is generally accepted that $(f_t)_{7\ days} = 0.7\ (f_t)_{28\ days}$; G_c and E_c also increase with age but not as drastically as f_t. Therefore, l_{ch} ($=E_cG_c/f_t^2$) should decrease with age. However there is no general agreement on how l_{ch} changes with age and the only published result is by Petersson (6) which gives $(l_{ch})_{28\ days}$ approximately equal to 0.7 times $(l_{ch})_{7\ days}$. Following this empirical result, we corrected the value of l_{ch} to 36.26 cm at 28 days and used this value to obtain the normalized curve shown in Fig. 17. (Actually, the shape of the σ–δ curve may also change with the age of the specimen. However little information is available to warrant further modification of our results). In general, the shape of the deduced σ–δ curve agrees well with those obtained by other investigators.

If we compare the relative values of f_t and G_c in Table 2, it can be seen that our specimens give a relatively high ratio for G_c/f_t. There are two plausible explanations. Firstly, our test is carried out at 7 days. With increasing age, the increase in f_t will be relatively more than the increase in G_c, resulting in a lower G_c/f_t ratio at 28 days. Secondly, the material we used is single-sized and without any finer particles besides cement. Since G_c is generally believed to increase with particle size, the lack of fine particles leads to a higher averaged particle size and a higher value for G_c in our specimens.

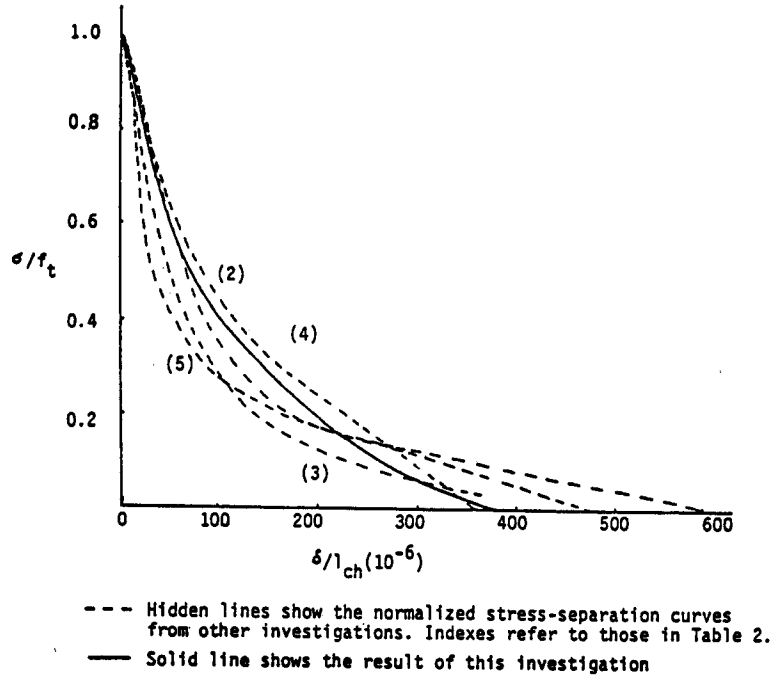

FIG. 17
Comparison of Different Tension-Softening Curves

A standard splitting test was performed on the same batch of mortar (with the same curing time) as used for the compact tension tests. The resulting splitting tensile strength was 3.65± 0.20 MPa. This is much higher than the value of 2.09 MPa (1.55-2.42 MPa) obtained for the σ–δ curve.

A plausible explanation for the discrepancy in f_t is the difference in strain rate used in the split test and that used in the compact tension specimen test. In the split test, the loading rate is about 1.037 MPa/min., in compliance with the ASTM standard. For the compact tension specimen, the average loading rate at the crack tip (assuming no stress concentration) for the second half of load increment before reaching the tensile strength is estimated to be 0.484 MPa/min.. Actually, when the tensile strength is approached, the stress-strain curve of the material tends to flatten off. The loading rate then can be much lower than the average. Moreover, the tensile strength obtained indirectly from the compact tension specimen is also affected by material ahead of the crack tip, where the strain rate is lower than that at the tip. The expected lower strain rate in the compact tension test may lead to a lower predicted tensile strength, based on correlation between strain rate and tensile strength observed by [13]. However, even the strain rate effect may not account fully for the discrepancy noted.

In future, direct tensile tests at appropriate loading rates will be performed as control tests. Only the tensile strength is needed, and the result may be used to supplement the data obtained in the indirect technique for the σ–δ curve described above.

To fully verify the applicability of the present technique, specimens of various sizes should be tested to see if the obtained σ–δ curve (and thus the value of G_c) is size-independent. Though this is not yet carried out, we expect the σ–δ curve to be size-independent as our testing technique does not involve any assumption of LEFM and the specimen size should therefore not affect our result.

CONCLUSIONS

The J-integral based experimental technique described in this paper has the advantages of requiring only small

specimens, a simple stroke controlled loading machine and is relatively stable. While the general agreement of the shape of the σ–δ curve with other investigations gives us more confidence in the application of this new experimental method, the disagreement of tensile strength with control test results calls for the need of further investigations. Currently, work is being done to refine the experimental technique based on 4 Point Bend specimens. The technique will be applied to study the fracture resistance of short-strand fiber-reinforced composites.

ACKNOWLEDGEMENT

The authors would like to thank S. Backer, H. Einstein and J. Germaine for valuable suggestions during the course of this work. We would also like to thank A. Rudolph for his technical assistance in the machine shop. The work was supported by the Sloan Foundation at MIT, and by a grant from the Solids and Geomechanics Program of the National Science Foundation.

REFERENCES

1 A. Hillerborg, Concrete Fracture Energy Tests Performed by 9 Laboratories According to a Draft RILEM Recommendation - Report to RILEM TC50-FMC, Report TVBM-3015, Lund Institute of Technology, Lund, Sweden (1983).
2 V.C. Li, Application of Fracture Mechanics to Cementitious Composites, Ed. S.P. Shah, p.431, Martinus Nijhoff Publishers, Dordrecht (1985).
3 V.C. Li and E. Liang, ASCE Journal of Engineering Mechanics 112, 566 (1986).
4 A. Hillerborg, Fracture Mechanics of Concrete, Ed. F.H. Wittmann, p.223, Elsevier Science Publisher, B.V., Amsterdam (1983).
5 R.H. Evans and M.S. Marathe, Materieux et constructions 1, 61 (1968).
6 P-E Petersson, Crack Growth and Development of Fracture Zones in Plain Concrete and Similar Materials, Report TVBM-1006, Lund Institute of Technology, Division of Building Materials (1981).
7 V.S. Gopalarathan and S.P. Shah, ACI Journal 82, 310 (1985).
8 H.W. Reinhardt, HERON, Delft Univ. of Technology Vol. 29, No. 2 (1984).
9 J.R. Rice, Fracture: An Advanced Treatise, Vol.2, p.191, Academic Press Inc., New York (1968).
10 C.M. Chan, Experimental Determination of Stress-Separation Curves for Cementitious Composite Materials, MS Thesis, MIT (1985).
11 A.R. Ingraffea and W.H. Gerstle, Application of Fracture Mechanics to Cementitious Composites, Ed. S.P. Shah, p.247, Martinus Nijhoff Publisher, Dordrech (1985).
12 S. Mindess and F. Young, Concrete, Prentice-Hall, Ltd., Englewood Cliffs (1981).
13 K. Komlos, ACI Journal 66, 111 (1969).